Microstructural Characterization and Strength Analysis of Hydride in Partially Recrystallized Annealed Cladding Tube Compared to CWSR Cladding

Donghyeon Son, Dahyeon Woo, Youho Lee*
Department of Nuclear Engineering, Seoul National University, Gwanak-ro 1, Gwanak-gu, Seoul 08826, Republic of Korea
**Corresponding author: leeyouho@snu.ac.kr*

Keywords: partial recrystallization, spent nuclear fuel, hydride, Zircaloy

1. Introduction

Due to the corrosion reaction between cladding and coolant, hydrogen enters Zircaloy cladding [1]. The absorbed hydrogen forms hydrides as the hydrogen concentration in the cladding exceeds the terminal solubility (TSS) limit of the Zircaloy. These precipitates play an important role in mechanical integrity since they can affect the ductility of the cladding so-called hydride embrittlement. The hydride embrittlement can lead to the failure of the Zircaloy cladding. It is especially crucial in spent fuel storage since the TSS limit is relatively low in low-temperature conditions. Therefore, understanding the hydride behavior is important to assess the safety of spent fuel storage.

Partially recrystallized annealed (PRXA) cladding was widely investigated because of its favorable creep and corrosion resistance. One of the factors that can affect the hydride formation is the microstructure of the Zr matrix. The alleviating effect of grain size on the hydride embrittlement was confirmed by numerous studies [2]. Therefore, there is a need to examine the different hydride behavior in various Zircaloy cladding with different microstructures, especially in different fabrication processes. This study unveils the distinctive hydride precipitation behavior of PRXA cladding based on optical microscopy (OM) and electron backscattered diffraction (EBSD). Comparisons with commercial cold work stress relieved (CWSR) cladding were presented. Radial hydride fraction (RHF), hydride characterization, and orientation relationship between Zr matrix and hydride were analyzed. Further mechanical approach through ring compression test (RCT) was conducted to assess the hydride embrittlement.

2. Experimental procedure

2.1. Material and hydrogen charging

PRXA Zr-1.1Nb-0.05Cu cladding tube with an outside diameter of 9.5 mm and thickness of 0.57 mm was used. The specimens were prepared by cutting the tube into 120 mm segments. 3-4 segments were put in a hydrogen charging apparatus. The apparatus was heated up to 400°C in a vacuum environment (10^{-6} Torr). Subsequently, hydrogen was charged targeting the concentration from 30 wppm to 700 wppm. After the hydrogen charging, the specimens were cooled down with a cooling rate of 0.5°C/min. After the hydrogen charging, the sample will be compared with CWSR Zr-Nb alloy investigated in past studies [2].

2.2. Microstructure characterization

Hydride morphology was observed using optical microscopy to analyze the hydride precipitation in a macroscopic manner. Mechanical polishing with SiC papers, diamond suspension, and colloidal silica suspensions was conducted for OM analysis.

The microstructure of the specimen was analyzed using EBSD. Field-emission scanning electron microscopes (FE-SEM, and model # JEOL JSM-7900F) equipped with an EBSD system (Oxford Instruments Symmetry). The accelerating voltage of FE-SEM was 20 kV. The EBSD results were analyzed with EDAX-OIM Analysis 8.6, AZtec 6.0, and AZtecCrystal 2.2. After the experiment, the hydrogen concentrations of the specimens were determined using the hydrogen analyzer (ELTRA ELEMENTRAC OH-p 2).

2.3. Mechanical testing

RCT was conducted to assess the ductility of the specimens. INSTRON-8516 with testing machine uniaxial load cell (1000 kN±0.05%) was used. The samples were prepared to a height of 8 mm. After the RCTs, hydrogen concentrations were determined using the hydrogen analyzer.

3. Results and Discussion

3.1. Microstructure of PRXA alloy

The microstructure of PRXA and CWSR cladding tubes were illustrated in Fig. 1. Average grain size of PRXA and CWSR alloy tubes were 1.27 μm, and 0.89 μm respectively. While the CWSR alloy shows an elongated grain structure, PRXA alloy shows the mixed structure of equiaxed grain and elongated grain resulting in partial recrystallization during the fabrication process. The orientation of the grain was colored in Fig. 1(a) and (b). PRXA alloy shows more disseminated orientation, while CWSR alloy shows a strong tendency of (01-10) plane.

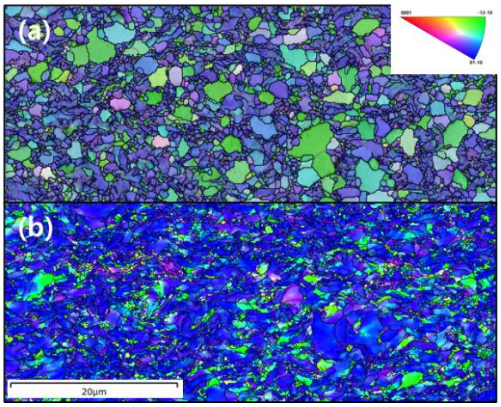

Fig. 1. Inverse pole figure (IPF) map of a) PRXA, b) CWSR cladding tube.

3.2. Macroscopic hydride morphologies

Hydride morphology was observed using OM (Fig. 2). Fig. 2(a1) and (a2) show the macroscopic morphologies with low hydrogen concentration under 50 wppm. Most of the hydrides are precipitated in a circumferential direction without applied stress. Therefore in Fig. 2(a2), interconnected hydrides were detected in reactor-grade CWSR alloy. However, even without applied hoop stress, radial hydride was detected in low-concentration PRXA specimens. RHFs were calculated using the image analysis software PROPHET [3]. The calculated RHF in PRXA cladding with low concentration was 23.1%, whereas the RHF of CWSR alloy with low concentration of hydrogen was negligible (Fig. 3(a1), (a2)). These significant amounts of radial hydride seem to affect the mechanical integrity of the cladding, however, Woo et al. [4] reported that the relationship between Strain energy density and RHF is no longer valid below 80 wppm of hydrogen contents. The additional mechanical analysis of low concentration specimen is given in section 3.5.

Above 180 wppm, hydrides were interconnected in a circumferential direction in PRXA cladding, which is similar to CWSR cladding with similar hydrogen concentration. A negligible amount of radial hydride was detected above 180 wppm of hydrogen content in both materials, as shown in Fig. 3(b)-(c).

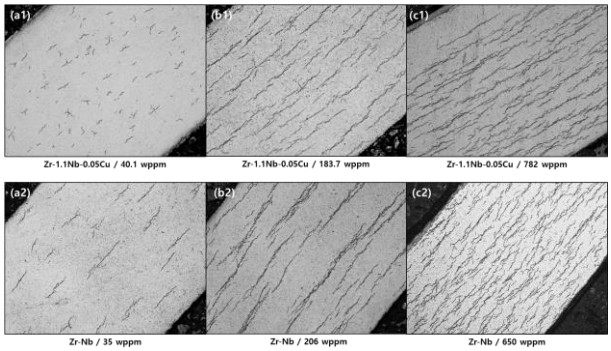

Fig. 2. OM images of PRXA and CWSR specimen with a) low hydride concentration under 50 wppm, b) intermediate hydride concentration about 200 wppm, c) high hydride concentration over 600 wppm

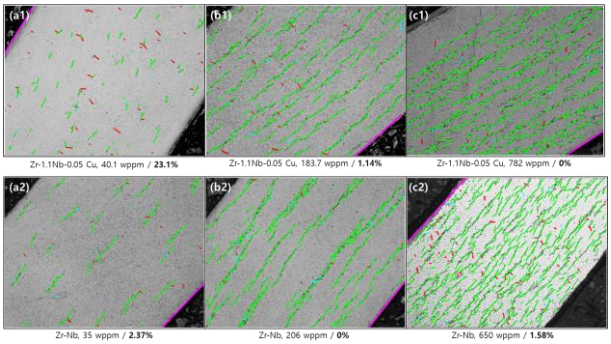

Fig. 3. RHF in PRXA and CWSR alloy with a) ~50 wppm, b) ~200 wppm, c) ~600 wppm

3.3. Hydride precipitation characteristics

Hydrides are classified into three categories based on the site of precipitation: inter-granular, intra-granular, and trans-granular hydrides. Inter-granular hydrides are precipitated in grain boundaries, while intra-granular and trans-granular hydrides are precipitated inside the grain. Trans-granular hydrides penetrate the grain. Fig. 4(a) shows the classification result of hydrides in PRXA. Inter-granular, intra-granular, and trans-granular hydrides are colored in yellow, red, and blue respectively. The crystal orientations of the Zr grain adjacent to the trans-granular hydrides are the same, which means that hydrides go through the grain.

Hydrides are usually nucleated in grain boundary in reactor-grade CWSR Zircaloy cladding [2] (Fig. 4 (b), step size 50nm). However, the number of hydrides precipitated in the grain boundary is relatively low in PRXA alloy compared to CWSR alloy (Fig. 4(a), step size 150nm). Therefore, there is more probability of nucleation inside the grain in PRXA alloy.

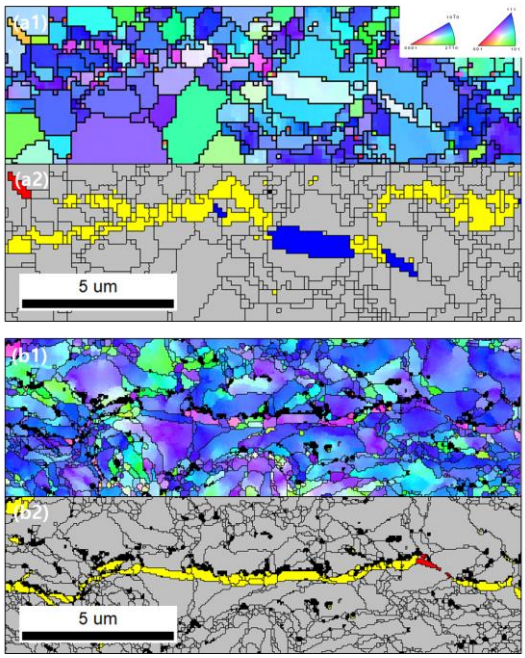

Fig. 4. IPF map and Phase map of zirconium hydride in a) PRXA, b) CWSR alloy

Calculated fractions of each hydride are shown in Fig. 5. Inter-granular hydrides are dominant in both PRXA alloy and CWSR alloy. In CWSR alloy, up to 90.6 % of inter-granular hydrides were detected. However, in PRXA alloy, inter-granular hydride fraction was 74.9%, and trans-granular hydrides are frequently detected (23.2%). The increased grain size affects the nucleation site in PRXA alloy.

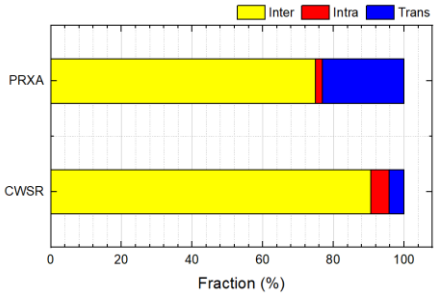

Fig. 5. Calculated fraction of classified hydrides.

3.4. OR and interface analysis

OR between Zr matrix and hydrides in PRXA alloy was analyzed through EBSD. Adding the angle between the interface and basal pole, whether the hydride is oriented in a circumferential or radial direction can be defined. The result is illustrated in Fig. 6. In CWSR alloy, which has a basal pole of Zr matrix tilted ~30° from the radial axis, the peak combination of two angles is (30°, 30°) [5]. In PRXA alloy, the weakened preference of the (30°, 30°) combination was detected (Fig. 6). The grain angle with radial axis varies in recrystallized grain from 10° to 50°, therefore high combination relationship from (30°, 30°) to (45°, 45°) was detected. Unlike previous studies that circumferential hydrides precipitate in the basal plane, the OR between the Zr matrix and hydride was usually incoherent.

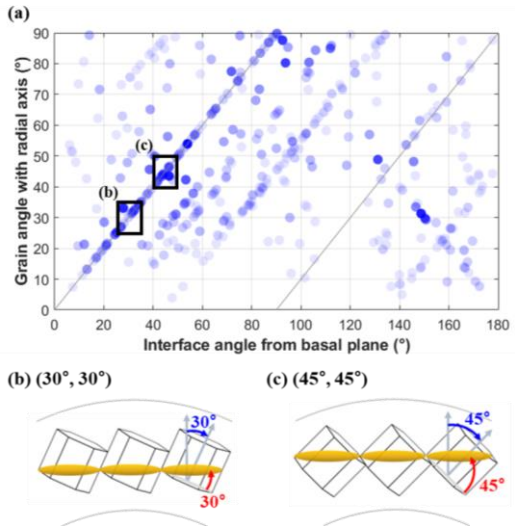

Fig. 6. a) Interface analysis of hydride in PRXA cladding tube and schematic image for the most general cases b) (30°, 30°), c) (45°, 45°)

3.5. Hydride embrittlement resistance of PRXA cladding

Fig. 7 shows a stress-strain curve between PRXA alloy and CWSR alloy with similar hydride concentrations. Compared to CWSR alloy, PRXA alloy exhibits more ductile behavior (i.e. increased elastic modulus). Usual load drop is determined by detecting the load drop larger than 30%, to calculate offset strain. In as-received CWSR alloy, major load drop was detected at ~94.1 MPa. After hydrogen charging, all the specimens showed a major load drop. However, a major load drop was not detected in the as-received PRXA alloy. Even after hydride precipitation, load drop didn't occur up to the strain of ~0.7 in 6 specimens among a total of 14 specimens. In some cases with load drop, a hill-shaped load drop was detected.

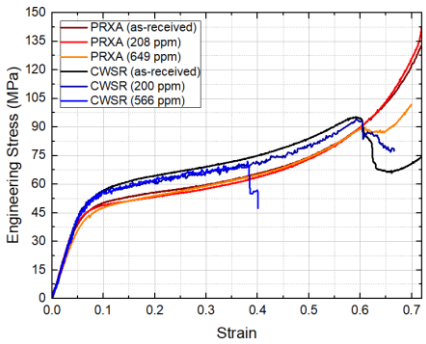

Fig. 7. Stress-strain curve of PRXA and CWSR cladding tube with various hydrogen concentrations.

Fracture strain was determined from the stress-strain curve (Fig. 8). The specimens with no load drop are marked with an X above the graph. PRXA alloy shows higher fracture strain compared to CWSR alloy. The significant amounts of radial hydride had no effect on the mechanical property in PRXA alloy. The ductile Zr matrix in PRXA cladding affects the increase of fracture strain. In a previous study, the ductile to brittle (DTB) transition of CWSR alloy was detected between 490 to 520 wppm of hydrogen content [2]. A decrease in fracture strain was detected in PRXA alloy near the same hydrogen concentration range. Nevertheless, the fracture strain of the material was similar to the fracture strain with low-concentration CWSR alloy.

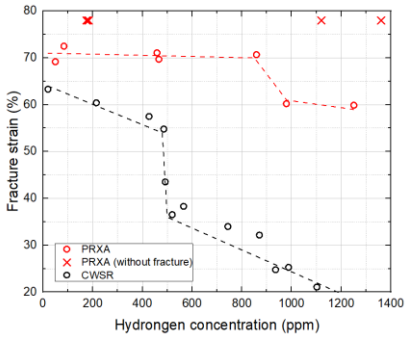

Fig. 8. Fracture strain-hydrogen concentration curve of PRXA and CWSR alloy.

4. Conclusions

Microscopic and mechanical analyses of hydride precipitation behavior in PRXA cladding tube compared to CWSR cladding were conducted. Key findings are as follows:

• High RHF was detected in PRXA cladding with low hydrogen concentration, however, in the hydrogen concentration above 180 wppm, the radial hydride was hardly detected.

• Hydride characterization and interface analysis of PRXA cladding were successfully conducted. PRXA cladding shows a higher amount of trans-granular hydrides than CWSR cladding. In interface analysis, the PRXA cladding shows a similar preference for (30°, 30°) angle combination with CWSR cladding. However, another peak region appears at (45°, 45°), resulting in the effect of recrystallized grain.

• Some radial hydrides in PRXA cladding may affect mechanical strength. However, PRXA cladding exhibits higher fracture strain compared to CWSR cladding, resulting in the alleviating mechanical strength of PRXA cladding. Hence, hydride precipitation in PRXA cladding up to the level of CWSR cladding used in current reactors can ensure the mechanical integrity of the cladding.

ACKNOWLEDGEMENT

This work was supported by the Nuclear Safety Research Program through the institute for Korea Spent Nuclear Fuel (iKSNF) using the financial resource granted by the Ministry of Science and ICT (MSIT) of the Republic of Korea [No. 2021M2E1A108598612].

REFERENCES

[1] B. Ensor, A. M. Lucente, M. J. Frederick, J. Sutliff, and A. T. Motta, "The role of hydrogen in zirconium alloy corrosion," Journal of Nuclear Materials, vol. 496, pp. 301-312, 2017.

[2] S. Kim, J.-H. Kang, and Y. Lee, "Hydride embrittlement resistance of Zircaloy-4 and Zr-Nb alloy cladding tubes and its implications on spent fuel management," Journal of Nuclear Materials, vol. 559, p. 153393, 2022.

[3] D. Kim, D. Kim, D. Woo, and Y. Lee, "Development of an image analysis code for hydrided Zircaloy using Dijkstra's algorithm and sensitivity analysis of radial hydride continuous path," Journal of Nuclear Materials, vol. 564, p. 153647, 2022.

[4] D. Woo and Y. Lee, "Understanding the mechanical integrity of Zircaloy cladding with various radial and circumferential hydride morphologies via image analysis," Journal of Nuclear Materials, vol. 584, p. 154560, 2023.

[5] J.-H. K. Dahyeon Woo, Youho Lee, "Advanced microstructural characterization of circumferential and radial hydrides in reactor-grade Zirconium cladding tube using EBSD and DSC," presented at the ANS Winter Conference and Expo., 2023.